Trim effect on the resistance of sailing planing hulls

Trim effect on the resistance of sailing planing hulls

Ignazio Maria VIOLA[1], Joshua ENLANDER[2] and Hamish ADAMSON[2]

[1] Institute for Energy Systems, School of Engineering, The University of Edinburgh, UK
[1] School of Marine Science and Technology, Newcastle University, UK

Corresponding author
Name: Ignazio Maria
Middle name: -
Surname: Viola
Tel: +44 131 650 5622
Fax: +44 131 650 6554
Email: i.m.viola@ed.ac.uk

Keywords

Hull resistance, towing tank, planing hull, dinghy, sport boat, skiff, pitch angle, trim angle

Abstract

Sailing skiffs are light-weight high-performance small boats of growing interest in competitive sailing. The present paper presents towing tank tests performed on the Aura skiff, which was a candidate for the 2016 Olympic games. Resistance, sink and trim were measured for different longitudinal positions of the crew weight and for Froude numbers (based on the boat's length over all) ranging from 0.30 to 1.03. For each test, detailed analysis of the measurement uncertainty was performed. The measured resistance was found in good agreement with the resistance computed with established empirical formulations developed for planing hulls. It was found that the optimum crew position moves from forward to aft when the Froude number increases. An incorrect longitudinal centre of gravity led to a maximum resistance penalty at Froude number around 0.4. These trends are in agreement with the sailor's experience and with measurements performed by other authors on large vessels.

1. Introduction

Sailing skiffs are high-performance lightweight competitive sailing craft. They have a large sail area compared to their displacement and, as such, they rely heavily on the weight of the crew to stabilize the vessel for optimal performance and also to avoid capsizing or pitch poling, where the bow buries itself in the water ahead of the vessel and the stern is lifted clear of the water up and rotates over the bow.

The Aura (Figure 1) is a modern skiff designed by Ovington Boats, a world leader in the construction of high performance dinghies. The Aura was designed in response to a request by the International Sailing Federation for a new women's Olympic skiff class. The result is a very lightweight, small platform skiff that requires very dynamic sailing to perform at its optimal level.

The typical practice in modern skiff sailing is that when sailing at high speeds the crew moves aft thereby lifting the bow area clear of the water to reduce hydrodynamic resistance and enhance handling. Figure 2 shows a typical high-speed condition with the crew position (CP) at about -40% of the length over all (LOA) from mid ship (MS), i.e. about 10% from the stern. The opposite is true when sailing at lower speeds, where the crew move closer to MS keeping the vessel as flat to the water as possible to reduce hydrodynamic resistance. For instance, Fig. 3 shows a typical low-speed condition with CP at about -20% from MS.

Use of towing tank model testing combined with computational fluid dynamics (CFD) is a common practice in sailing yacht design. Conversely, small dinghies are normally designed with low budgets: towing tank tests and CFD are rarely used while full-scale prototype field testing is more affordable than for large yachts. However, full-scale tests are difficult to interpret due to the variable environmental conditions. Successful examples of full-scale measurements are those reported by Frank Bethwaite (1993). A transverse beam connects three parallel boats. The dinghy being tested is attached to one end of the beam, the towing powerboat is attached at the middle of the beam and a reference dinghy is attached to the other end of the beam. This technique was also adopted by

Watin (2007) to test the effect of different pitch angles on the resistance of a 49er-class skiff, which was designed by Julian Bethwaite, Frank's son. Watin found that sailing with a lower pitch angle at low speed and a higher pitch angle at high speed allows a reduction of the total resistance.

As far as known by the present authors, this paper presents the first towing tank test on sailing skiffs. However, there has been extensive experimental and numerical investigation on the hydrodynamics of planing vessels in general, for instance, the systematic prismatic model testing undertaken by Savitsky (1964), by Savitsky and Brown (1976) and more recent hard chine test series undertaken by Taunton et al. (2010). Thornhill et al. (2003) conducted resistance tests to validate CFD results on a model that was similar to the Aura in regards to low deadrise angle, i.e. with relatively flat bottom that sharply turns at the side of the hull. The model was ballasted at different static trim angles and it was found that lower static trim angles initially reduce resistance but at higher speeds the resistance is greater than cases with higher static trim angles. While Thornhill et al. tested a 1:8th scale model of a 15 tonne vessel, in the present paper a 1:4th scale model of a 90 kg boat is tested. Despite of the very different type of vessel, similar conclusions on the effect of the static trim angles on the resistance was achieved. The resistance of planing hulls was computed with CFD by several authors who found good correlation with towing tank data. For instance, Caponnetto (2000 and 2001) and Azcueta (2003) showed that a Reynolds-averaged Navier-Stokes approach can be used to accurately predict the hull resistance at high Froude numbers modelling the free surface with a volume-of-fluid technique.

2. Experimental Method

2.1. Model

In the present work, the hull shape was a 1:4 scale model of the Aura. It was constructed from carbon fibre using a computer numerical control milled mould. A carbon fibre base plate was fixed to the inside of the model such that its top surface was parallel with the still waterline defined by the

design waterline. The hull surface was marked with the still waterline and 12 transverse sections, from Station 0 at the aft extreme of the model to Station 11 at the forward extreme of the model. Also 11 half stations were marked midway between the full stations. The marked transverse sections are visible in Fig. 4, which shows a photograph of the Aura model towed in the towing tank.

2.2. Experimental Setup

The testing was undertaken in the Hydrodynamics Laboratory of the School of Marine Science and Technology, Newcastle University, UK. The facility features a towing tank of LxBxD, 37x3.7x1.25 m and uses a monorail carriage assembly on which all data acquisition and processing equipment is fitted.

Figure 5 shows the experimental setup. The longitudinal centre of gravity of the model (LCG_0) was found by balancing the model longitudinally on a knife edge fulcrum. An aluminium towing plate was then attached to the carbon fibre base plate such that its central seating pin was on the intersection of LCG_0 and the boat symmetry plane.

Full-scale Reynolds numbers based on LOA ranged from $1.0 \cdot 10^7$ to $3.5 \cdot 10^7$ for the tested conditions, thus the boundary layer on the hull is mostly turbulent. Conversely, in model scale, Reynolds number ranged from $1.2 \cdot 10^6$ to $4.3 \cdot 10^6$ leading to a larger region of laminar boundary layer. Therefore, a $2.5\ \mathrm{mm}$ probe entering the water $0.1\ \mathrm{m}$ from the bow at the vessels still water condition was used as turbulence generator (Fig. 5).

A Gifford dynamometer was used (Fig. 6) to measure the port and starboard drag forces and forwards and aft side forces using four thin-wall load cells; while the longitudinal angle of the model (pitch) was measured using a potentiometer. The Gifford dynamometer was connected to a post which measured the vertical displacement of the model (heave) using a potentiometer. The carriage velocity was measured using an optical rotating wheel mechanism. The seating hole of the Gifford dynamometer base plate was seated on the seating pin of the towing plate. The Gifford

dynamometer allows free roll motion of the model via a roll pin. For these experiments the pin was locked thereby eliminating the roll action. Conversely the model was allowed to pitch freely. A plastic splash guard and cover were attached to the deck opening during testing to reduce the risk of flooding at high pitch angles and velocities.

The full-scale Aura skiff weighed $90\ \mathrm{kg}$ and tests were performed for a crew of two sailors of $137\ \mathrm{kg}$ in total. In a 1:4th model scale, boat and crew would result in $1.406\ \mathrm{kg}$ and $2.134\ \mathrm{kg}$ respectively, and $3.541\ \mathrm{kg}$ in total. The model was built as light as possible while still retaining the required strength and stiffness for model testing resulting in a weight of $1.794\ \mathrm{kg}$. In addition to this, the Gifford dynamometer and heave post weighed $4.609\ \mathrm{kg}$. Therefore a counterbalance system was used acting through the heave post. In order to model different longitudinal positions of the crew, the counter balance weight was chosen so as to allow a movable ballast weight of 2kg to trim the model. A weight breakdown is shown in Table. 1.

At the start of each test day the model was set to its still waterline by placing the $2\ \mathrm{kg}$ ballast on the Gifford dynamometer thus contributing to the displacement without applying a pitching moment. In order to take into account the friction within the counterbalance system and the surface tension of the water, the model was intermittently disturbed in heave until a no change in vertical position was measured between disturbances. The ballast was then moved to the test position and a preliminary run was made to allow the model to settle. Then data acquisitions (DAQ) of velocity, resistance, heave and pitch were zeroed and the first measured run was made. DAQ's were also re-zeroed before each successive run.

2.3. Test Matrix

Five ballast positions were tested each resulting in a change of the total longitudinal centre of gravity LCG (including model, dynamometer, post and ballast), which is referenced from MS as a percentage of LOA with positive measurements forward. Each ballast position was tested on a separate day and it was attempted to replicate the same test velocities (V) on each day. However

the analogue nature of the carriage velocity control system resulted in a different set of velocities every day. Also the necessary waiting time for the tank to settle between each run resulted in a different number of tests that could be run each day. The ballast positions tested and the corresponding total LCG of the vessel are presented in Table 2. The model-scale length water line (LWL) in static condition is also presented for each LCG.

Additional experiments were performed to assess the measurement uncertainty. Also, the last tested condition with the ballast at -46% was repeated 9 days after the original to determine the repeatability of the results. Table 3 shows which speed and corresponding Froude number (Fr, based on LOA) was tested each day.

2.4. Experimental Uncertainty

In this section the methods used to determine the precision of the experiment are discussed. Where possible, the Recommended Procedures and Guidelines (RP&G) of the International Towing Tank Conference (ITTC) were followed.

For each i-th parameter, the uncertainty (U_i) was broken down into j components ($U_{i,j}$). The analysed parameters are the static wetted surface area (S) at the design waterline, the velocity (V), the density of water (ρ), the total resistance (R_T) and the total resistance coefficient ($C_T = R_T/(1/2\ \rho V^2\ S)$). The total uncertainty of each parameter was found as the root sum square of the components (L_2 norm), Eq. (1):

$$U_i = \sqrt{U_{i,1}^2 + U_{i,2}^2 + \cdots + U_{i,n}^2} \quad (1)$$

The model was constructed within the accuracy recommended by the ITTC RP&G for Ship Models (ITTC, 2002) resulting in a model error of ±1 mm giving an uncertainty in the measurement of the displacement and draught and thus an uncertainty in the wetted surface area ($U_{S,MOD}$). The model, Gifford dynamometer, heave post, crew weights and counterweight were weighed using a balance

with an uncertainty of 10^{-3} kg thus giving an uncertainty in the displacement and in the wetted surface area ($U_{S,BAL}$). The total wetted surface area uncertainty (U_S) was calculated with Eq. (1).

The DAQ uncertainties were calculated using the Type A uncertainty method described by the Guide to the Expression of Uncertainties in Experimental Hydrodynamics of the ITTC RP&G (ITTC, 2008a), Eq. (2):

$$U_{i,DAQ} = \frac{S_i}{\sqrt{n}} \quad (2)$$

Where S_i is the standard deviation of the measured data and n is the number of data points.

The calibration uncertainty of the velocity measurement device ($U_{V,CAL}$) was determined by timing the carriage for 10 m after acceleration using a timer with a minimum count of 10^{-3} s. The DAQ uncertainty ($U_{V,DAQ}$) was determined by the Type A uncertainty method, shown in Eq. (2). The total velocity uncertainty (U_V) was calculated with Eq. (1).

The load cells were calibrated using Newton weights with an uncertainty of 0.001% thus causing a calibration uncertainty in the measurement of the total resistance ($U_{R_T,CAL}$). The curve fitting uncertainty ($U_{R_T,FIT}$) was determined as the standard error estimate of the calibration data, Eq. (3):

$$U_{R_T,FIT} = \sqrt{\frac{\sum r^2}{(n-2)}} \quad (3)$$

Where r are the residuals of the curve fit.

The DAQ uncertainty of the total resistance ($U_{R_T,DAQ}$) was determined by the Type A uncertainty method, Eq. (2). The uncertainty due to misalignment of the model ($U_{R_T,MIS}$) was determined by testing the model at maximum port and starboard misalignments. The total resistance uncertainty (U_{R_T}) was calculated with Eq. (1).

The thermometer used to measure tank temperature was found to have an uncertainty $U_t = 0.75°C$. The density uncertainty (U_ρ) was calculated with the formula provided by the ITTC RP&G for Density and Viscosity of Water (ITTC, 1999).

The uncertainty in the total coefficient of resistance (U_{C_T}), was determined following the ITTC RP&G in Resistance Towing Tank Tests (2008b), Eq. (4):

$$\left(\frac{U_{C_T}}{C_T}\right)^2 = \left[\frac{\left(U_t \frac{\delta\rho}{\delta t}\right)}{\rho}\right]^2 + \left(\frac{2U_V}{V}\right)^2 + \left(\frac{U_{R_T}}{R_T}\right)^2 + \left(\frac{U_S}{S}\right)^2 \quad (4)$$

Where $\delta\rho/\delta t$ is the density/temperature gradient. ITTC RP&G (ITTC, 1999) defines density for $g = 9.81\ \mathrm{m/s^2}$ as Eq. (5):

$$\rho = 1000.1 + 0.0552\,t + 0.0077\,t^2 + 0.00004\,t^3 \quad (5)$$

Therefore $\delta\rho/\delta t$ was derived as Eq. (6):

$$\frac{\delta\rho}{\delta t} = 0.0552 - 0.0154\,t + 0.000120\,t^2 \quad (6)$$

Uncertainties are presented in the form of error bars in Section 3.2 for each measurement, while Table 4 shows an example of uncertainty break down for a test performed at $1.8\ \mathrm{m/s}$ and $LCG = -24\%$. The example shows that the uncertainty of the resistance coefficient is of the order of 10% and it is mostly due to $U_{R_T,DAQ}$. An additional source of uncertainty, which has not been accounted for, is the misalignments of the model with respect to the longitudinal axis of the tank. For each test a small side force, smaller than 5% of the resistance, was measured, suggesting a minimal misalignment potentially leading to an induced drag of the order of 1% of the total resistance.

2.5. Sensitivity

A sensitivity analysis was undertaken to determine which parameters most significantly affect the calculation of the total resistance coefficient.

Each parameter was arbitrarily and independently increased by a value of one and the resulting change in C_T was used to calculate the sensitivity coefficient (θ_i) as Eq. (7):

$$\theta_i = \frac{\delta C_T}{\delta i} \quad (7)$$

Where δi is the percentage change of the i-th parameter and δC_T is the percentage change in C_T.

For example, for $LCG = -24\%$ and $Fr = 0.52$, resistance and resistance coefficients are $R_T = 4.51\ N$ and $C_T = 15.50 \cdot 10^{-3}$, respectively. If R_T is arbitrary increased by 1N, then $\delta R_T = 1/4.51 = 22.16\%$ and $\delta C_T = 3.43 \cdot 10^{-3}/15.50 \cdot 10^{-3} = 18.14\%$ (Table 5).

Table 5 shows that V has the most significant effect on C_T. In particular, a 1% change of V leads to a -2.56% change in C_T. Therefore particular care was taken to keep the velocity uncertainty value low, resulting in $U_V = 0.009\%$ for the example test run shown in Table 4.

3. Results

3.1. Results overview

The experimental measurements showed good consistency: a relatively small measurement scatter was found and the identification of clear trends for different positions of the 2 kg ballast was possible. The following results are presented without the use of any fitting or smoothing functions.

An overview of the results is presented in Fig. 7, where the model-scale resistance is mapped for the range of tested LCG and V. Also included are the full-scale resistance $\left(R_{T_{FS}}\right)$ and velocity (V_{FS}) computed with the Huges-Prohaska method and the 1957 ITTC model correlation line (ITTC, 2008c).

In particular, the full-scale resistance coefficient $\left(C_{T_{FS}}\right)$ was computed from Eq. (10), where k is the form factor measured with the Prohaska method, while the coefficients of friction for full scale $\left(C_{F_{FS}}\right)$ and model scale (C_F) were derived from Eq. (11) and (12) taken from the 1957 ITTC model correlation line (ITTC, 2008c).

$$C_{T_{FS}} = C_T - (1+k)\left(C_F - C_{F_{FS}}\right) \quad (10)$$

$$C_F = \frac{0.075}{(\log_{10} Re - 2)}, \quad Re = \frac{V\ (LOA)}{\nu} \quad (11)$$

$$C_{F_{FS}} = \frac{0.075}{(\log_{10} Re_{FS} - 2)}, \quad Re_{FS} = \frac{V_{FS}\ (LOA_{FS})}{\nu} \quad (12)$$

Where ν is the kinematic viscosity.

Figure 7 shows that at low-speed regimes, LCG closer to MS allows lower R_T than LCG farther aft, therefore the optimal LCG appears to be farther forward than those which were tested. Conversely, at high-speed regimes, there seems to be an optimal LCG position between -21% and -24%. These trends are in agreement with the sailing practice, where the crew move aft to reduce the resistance when the boat speed increases. These are also in agreement with the findings of Thornhill et al. (2003) on the 1:8th-model-scale 15-tonnes vessel and with the full-scale measurements of Watin (2007) on the 49er-class skiff.

The full-scale Fr range is higher than the tested Fr range; however the range of tested conditions covers the typical three displacement regimes of a high-speed craft from the displacement regime to the fully planing regime. At low speed (roughly $Fr < 0.4$), an inviscid Kelvin wake was observed and the highest wave elevations were found at the bow and stern. In the semi-displacement regime (roughly $0.4 < Fr < 0.6$), only the second half of the boat length was wet and the generated wave length was about twice the wetted boat length. In this Fr range, a very large stern wave was generated associated with a high resistance coefficient. In the fully planing regime (roughly $Fr > 0.6$), the wake was significantly thinner and the stern trough was smaller.

Three additional tests were performed at low speeds in order to extrapolate the form factor using the method suggested by Prohaska (1966). Figure 8 shows the three measurements and the linear fit. The extrapolated form factor is $k = 0.07$.

3.2. Resistance Coefficient

Figure 9 shows C_T with error bars showing the uncertainty. The results for the repeat of the -29% test case are also presented. The -29% and -24% cases were verified using the empirical formula developed by Savitsky (1964) and Savitsky and Brown (1976) for planing hulls and results are presented. The repeated case shows a good correlation to the original test, though differences from the Savitsky prediction are observed from $Fr \cong 0.6$ to $Fr \cong 1.0$. possibly due to the significant longitudinal curvature of the keel line of the Aura.

At low Fr, LCG farther from MS causes greater C_T than with LCG closer to MS; at higher Fr the inverse occurs. In particular the minimum C_T is achieved with LCG successively moving aft from -13% to -29% when Fr increases. Table 6 shows the cross overs between the tested LCG conditions computed interpolating the measured data with splines. Up to $Fr = 0.81$, the minimum C_T is achieved for the most forward tested position of LCG (-13%). For $Fr > 0.81$ the minimum C_T can be achieved for an intermediate LCG between -13% and -15%. Table 6 shows further cross overs until $Fr > 1.09$ when the most aft LCG (-29%) data allows the minimum C_T.

It must be noted that each curve in Fig. 9 does not represent a fixed longitudinal crew position in real sailing conditions. In fact, the sail aerodynamic forces applied at the sail's centre of effort lead to a pitch moment, which pushes the bow down. In steady conditions (i.e. when sailing at a constant velocity), the thrust is equal to the opposite of the resistance and the pitch moment arm can be assumed as the height of the geometrical centre of the sailplan. For each tested condition, the modelled crew position can be computed considering that the pitch moment due to the 2 kg ballast is the sum of the pitch moments due to the sails and the crew. Figure 10 shows C_T versus Fr for two different values of fixed crew positions. The trends confirm that the higher the Fr, the more aft crew

positions allow lower resistance. In particular, for $Fr > 0.85{\sim}0.90$, a shift of the crew position from -35% to -45% allows a reduction of the resistance.

3.3. Heave

Figure 11 shows the heave for each test case. The heave increases with Fr and decreases with LCG. As for the resistance coefficient the repeated test case with $LCG = -29\%$ is presented. Two repeated measurements at high Fr were discounted due to a malfunction of the heave measurement potentiometer that occurred during these test runs.

It can be seen from Fig. 11 that as the crew ballast is moved further aft, the onset of heaving of the vessel occurs at lower a Fr due to the increased angle of attack.

3.4. Pitch

Figure 12 shows the pitch of each test case. All of the cases exhibit the same increase in pitch until an initial hump is reached after which the pitch continues to increase. The $LCG = -29\%$ case and its repeat show a second hump where the high pitch led to mild porpoising. Using the formula suggested by Savitsky (1964), porpoising was expected to occur for pitch angles greater than $4.5°$. This is consistent with the experimental results. In fact, for pitch angles greater than $4.5°$, oscillations in the pitch measurement were observed resulting in a change of the pitch slope for increasing Froude numbers.

4. Conclusions

Towing tank tests were performed on a 1:4 scale model of a high-performance skiff to determine whether the longitudinal crew position affects the performance of such planing craft. Tests were performed for a range of Froude number up to 1.03 and for different positions of the longitudinal centre of gravity. Analysis of uncertainty showed that the uncertainty on the measured resistance coefficient was up to 12% within a 95% confidence level at lower Froude numbers. In all cases the

uncertainty decreased as velocity increased resulting in uncertainties in the measured resistance coefficient reducing to 6% within a 95% confidence level.

It was found that the minimum resistance is achieved for fore crew positions at lower Froude numbers and aft crew positions at higher Froude numbers. Without taking into account of the aerodynamic pitch moment, between Froude numbers from 0.81 and 1.09 (extrapolated value), the optimum longitudinal centre of gravity moves 16% of the boat length backwards (from -13% to -29% from mid ship). Forward positions of the centre of gravity led to higher heave and pitch angles for every tested condition. When the aerodynamic pitch moment is taken into account, the optimum crew position is showed to be around -40% of the boat length from mid ship, forward this position for lower Froude numbers and aft this position for higher Froude numbers.

5. Acknowledgements

The Aura design and model manufacture was completed by Mr Peter Hobson, Ovington Boats (North Shield, UK), who is greatly acknowledged by the authors.

6. References

Azcueta R. (2003). Steady and Unsteady RANSE Simulations for Planing Crafts. *In the proceedings of The 7th International Conference on Fast Sea Transportation* (FAST2003), 7th-10th October, Ischia, Italy.

Bethwaite, F., (1993). High Performance Sailing: Faster Racing Techniques, Waterlines Books, UK.

Caponnetto M. (2000). Numerical Simulation of Planing Hulls. *In the proceedings of The 3rd Numerical Towing Tank Symposium* (NuTTS2000), 9th -13th Sep, Tjarno, Sweden.

Caponnetto M. (2001). Practical CFD Simulations for Planing Hulls. *In the proceedings of The 2nd International Conference on High-Performance Marine Vehicles* (HIPER2001), 2nd-5th May, Hamburg, Germany.

Prohaska, C.W. (1966). A Simple Method for Evaluation of Form Factor and the Low Speed Wave Resistance, *In the proceedings of The 11th International Towing Tank Conference*, 11th-20th October, Tokyo, 65-66.

ITTC (1999), Density and Viscosity of Water. ITTC Recommended Procedures and Guidelines, Procedure 7.5-02-01-03, Revision 00.

ITTC (2002), Ship Models. ITTC Recommended Procedures and Guidelines, Procedure 7.5-01-01-01, Revision 01.

ITTC (2008a), Guide to the Expression of Uncertainties in Experimental Hydrodynamics. ITTC Recommended Procedures and Guidelines, Procedure 7.5-02-01-01, Revision 01.

ITTC (2008b), Guidelines for Uncertainty Analysis in Resistance Towing Tank Tests. ITTC Recommended Procedures and Guidelines, Procedure 7.5-02-02-02, Revision 01.

ITTC (2008c), Testing and Extrapolation Methods, High Speed Marine Vehicles, Resistance Test. ITTC Recommended Procedures and Guidelines, Procedure 7.5-02-05-01, Revision 02.

Savitsky, D. (1964). Hydrodynamic Design of Planing Hulls. *Marine Technology*, 1(1): 71-95.

Savitsky, D., Brown, P.W. (1976). Procedure for Hydrodynamic Evaluation of Planing Hulls in Smooth and Rough Water. *Marine Technology*, 13(4): 381-400.

Taunton, D.J., Hudson, D.A., Shenoi, R.A. (2010). Characteristics of a Series of High Speed Hard Chine Planing Hulls – Part 1: Performance in Calm Water. *Transactions of the Royal Institution of Naval Architects Part B: International Journal of Small Craft Technology,* 152(2): 55-74

Thornhill, E., Oldford, D., Bose, N., Veitch, B., Liu, P. (2003). Planing Hull Performance From Model Tests. *International Shipbuilding Progress,* 50(1-2): 5-18

Viola, I. M, Flay, R. G. J., Ponzini, R. (2012). CFD Analysis of the Hydrodynamic Performance of two Candidate America's Cup AC33 Hulls. *Transactions of the Royal Institution of Naval Architects Part B: International Journal of Small Craft Technology*, 154(1): 1-12

Watin, S. (2007). 49er Performance Enhancement. Supervisor: J. Bethwaite. Internship report, 52 pp., Ecole Polytechnique, Palaiseau, France.

Figure 1
Click here to download high resolution image

Figure 2
Click here to download high resolution image

Figure 3
Click here to download high resolution image

Figure 4
Click here to download high resolution image

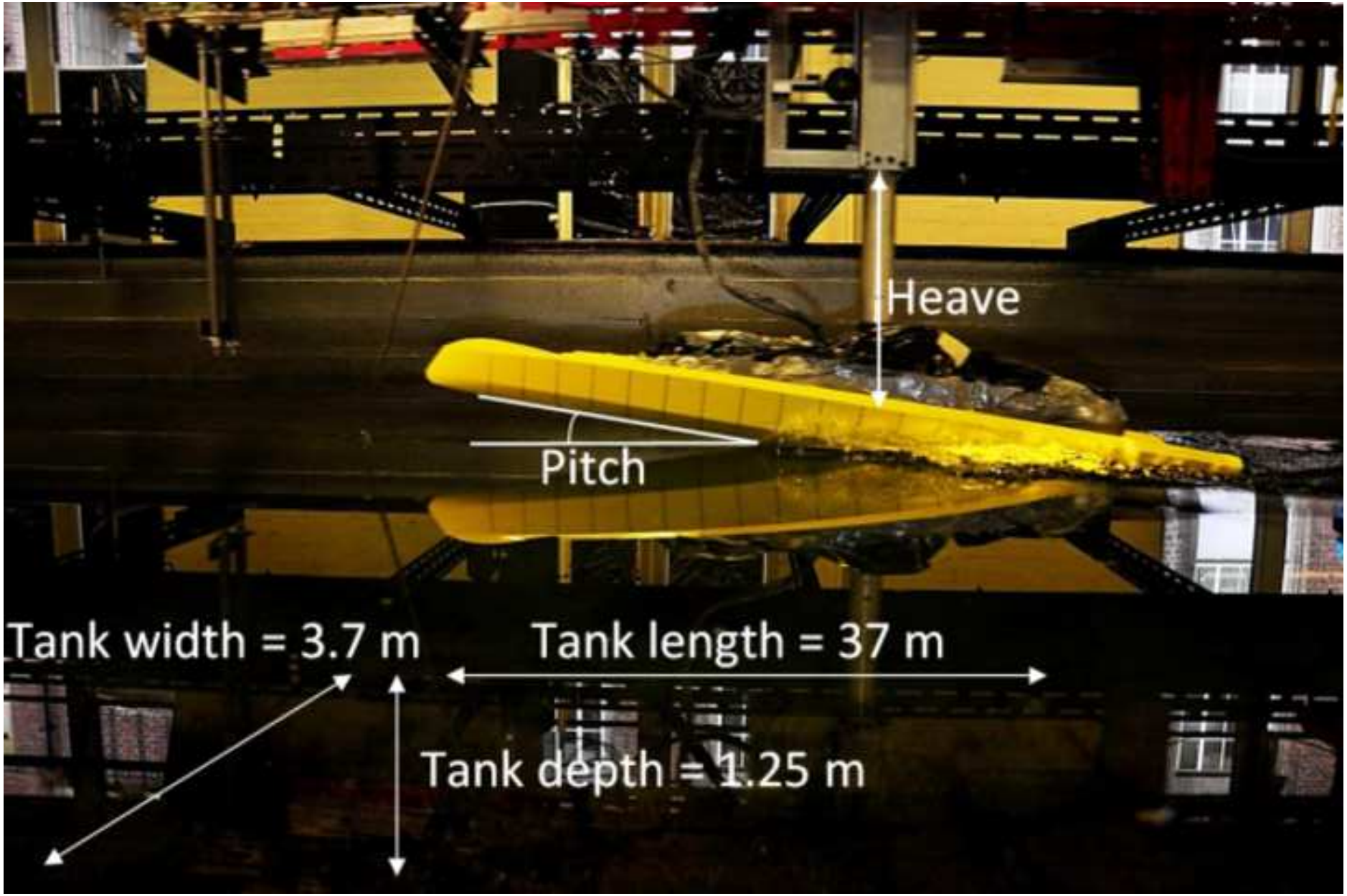

Figure 5
Click here to download high resolution image

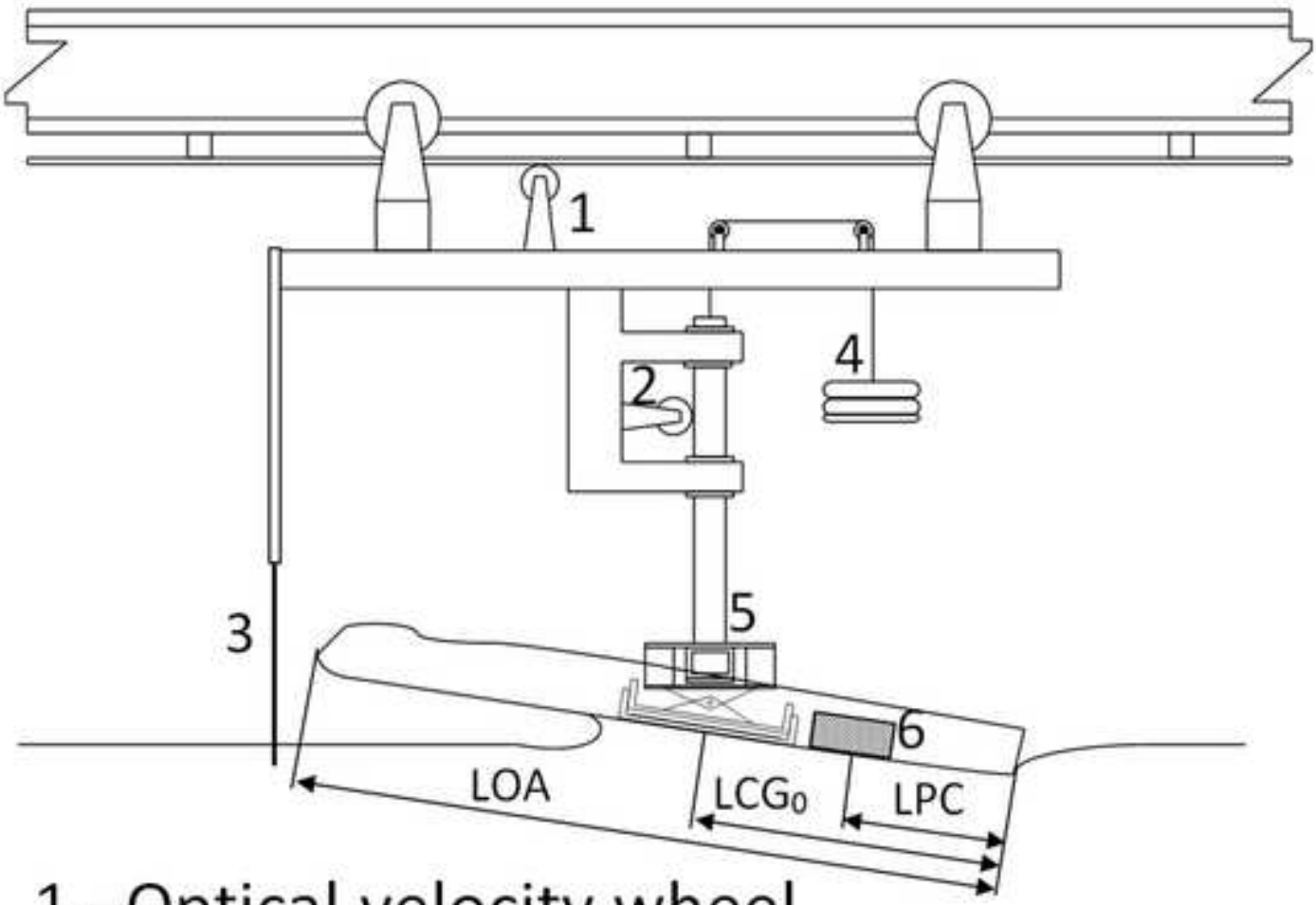

1 –Optical velocity wheel
2 – Heave wheel
3 – Turbulence stimulator
4 – Counter weight
5 – Gifford dynamometer
6 – Ballast

Figure 6
Click here to download high resolution image

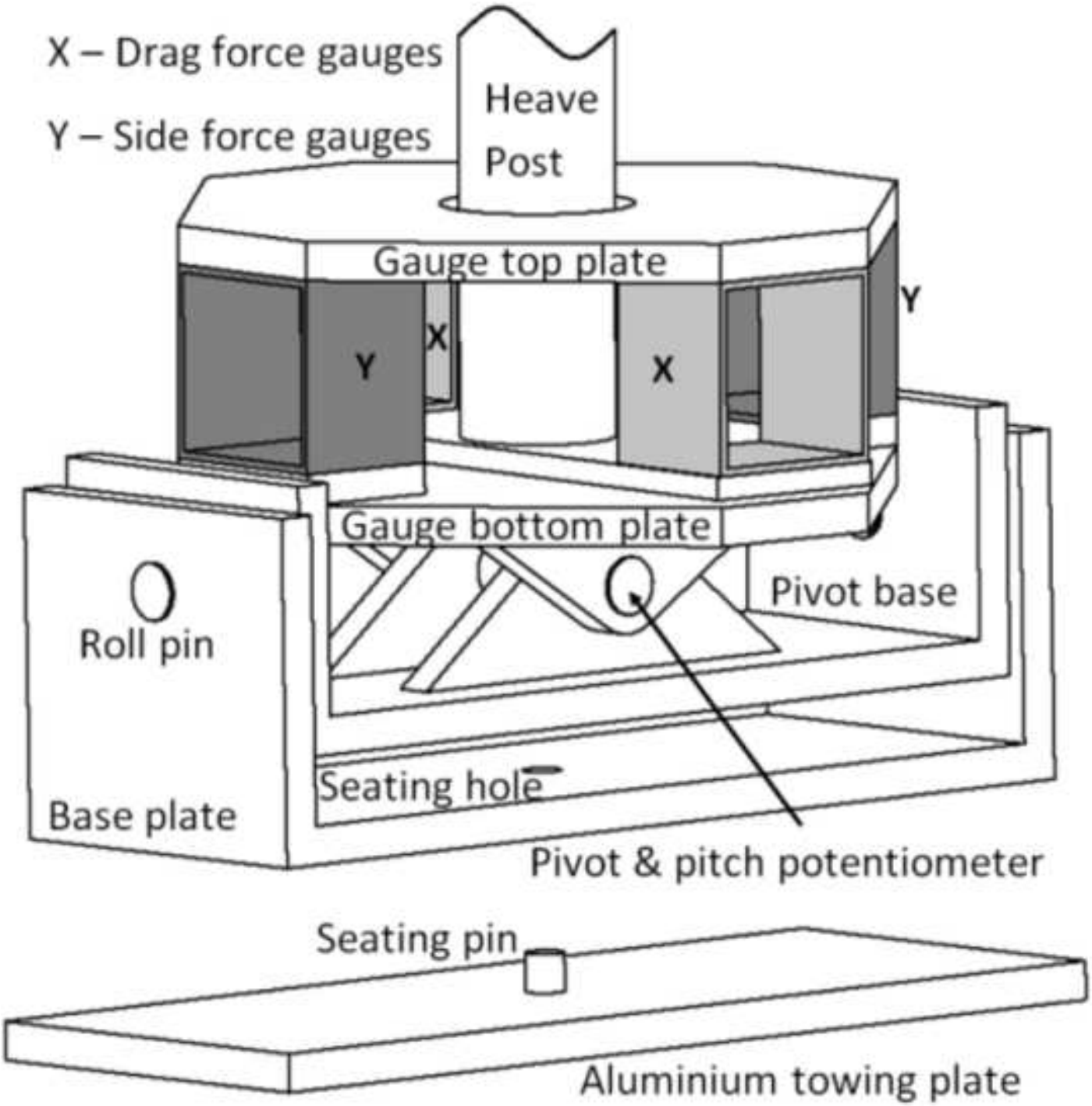

Figure 7
Click here to download high resolution image

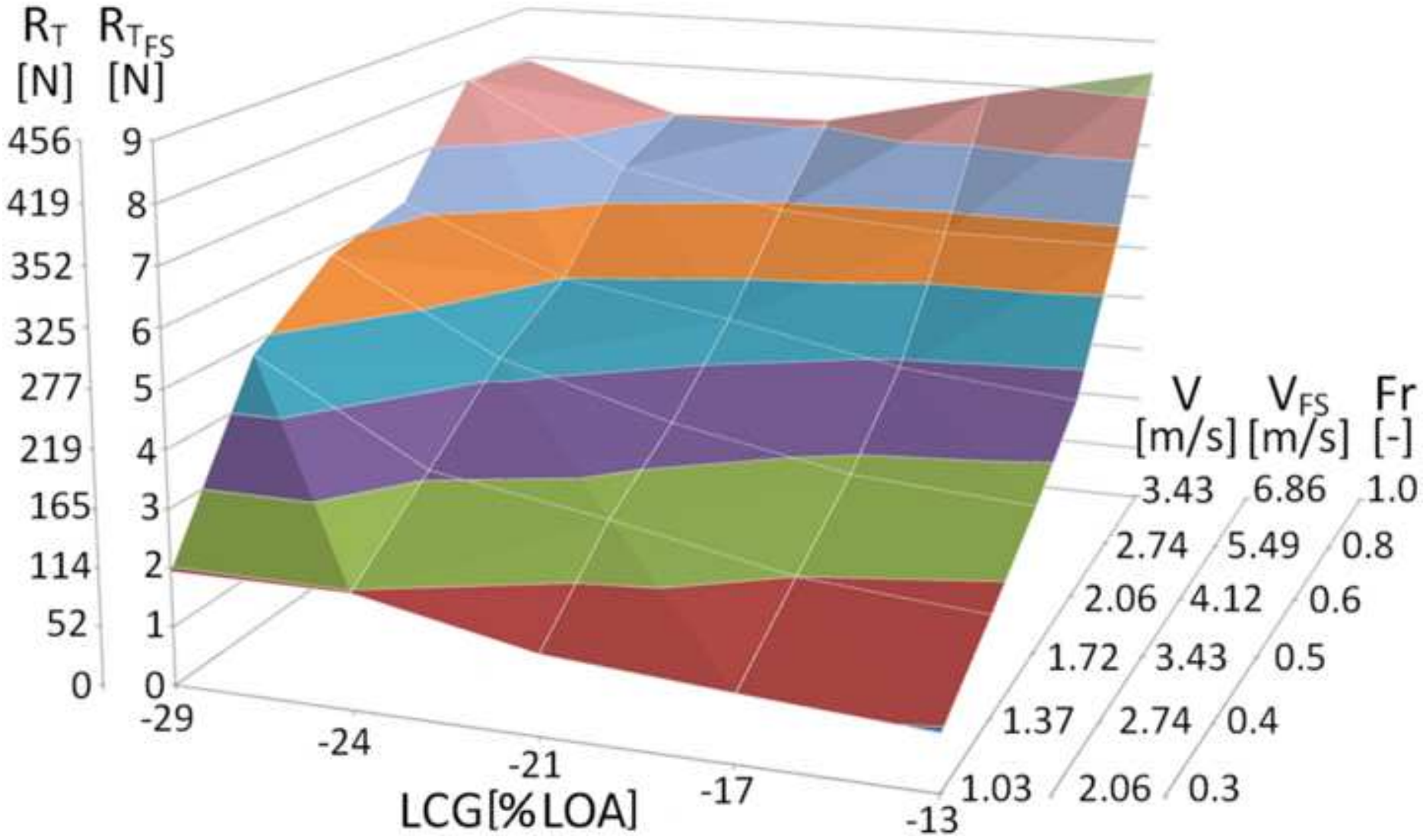

Figure 8
Click here to download high resolution image

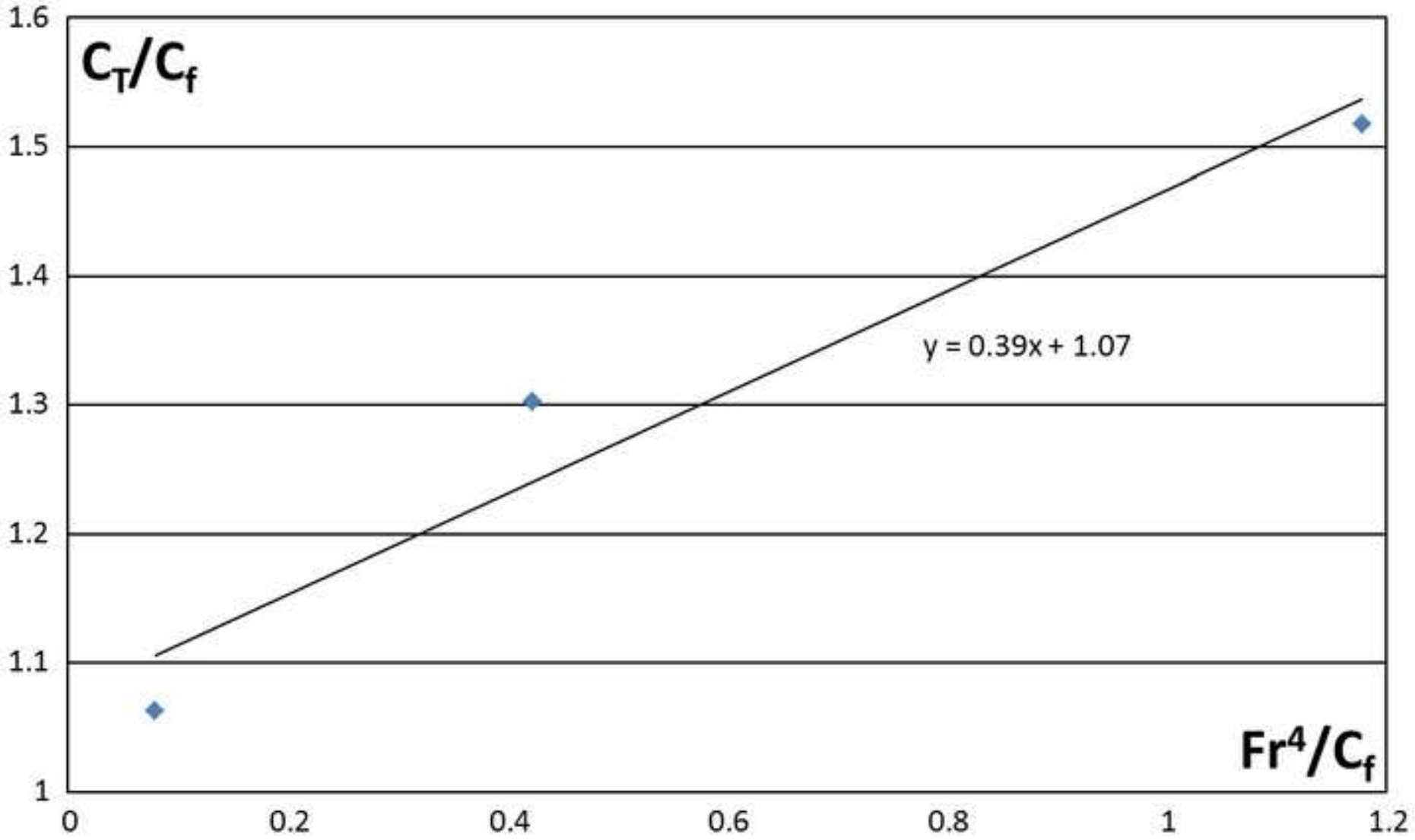

Figure 9
Click here to download high resolution image

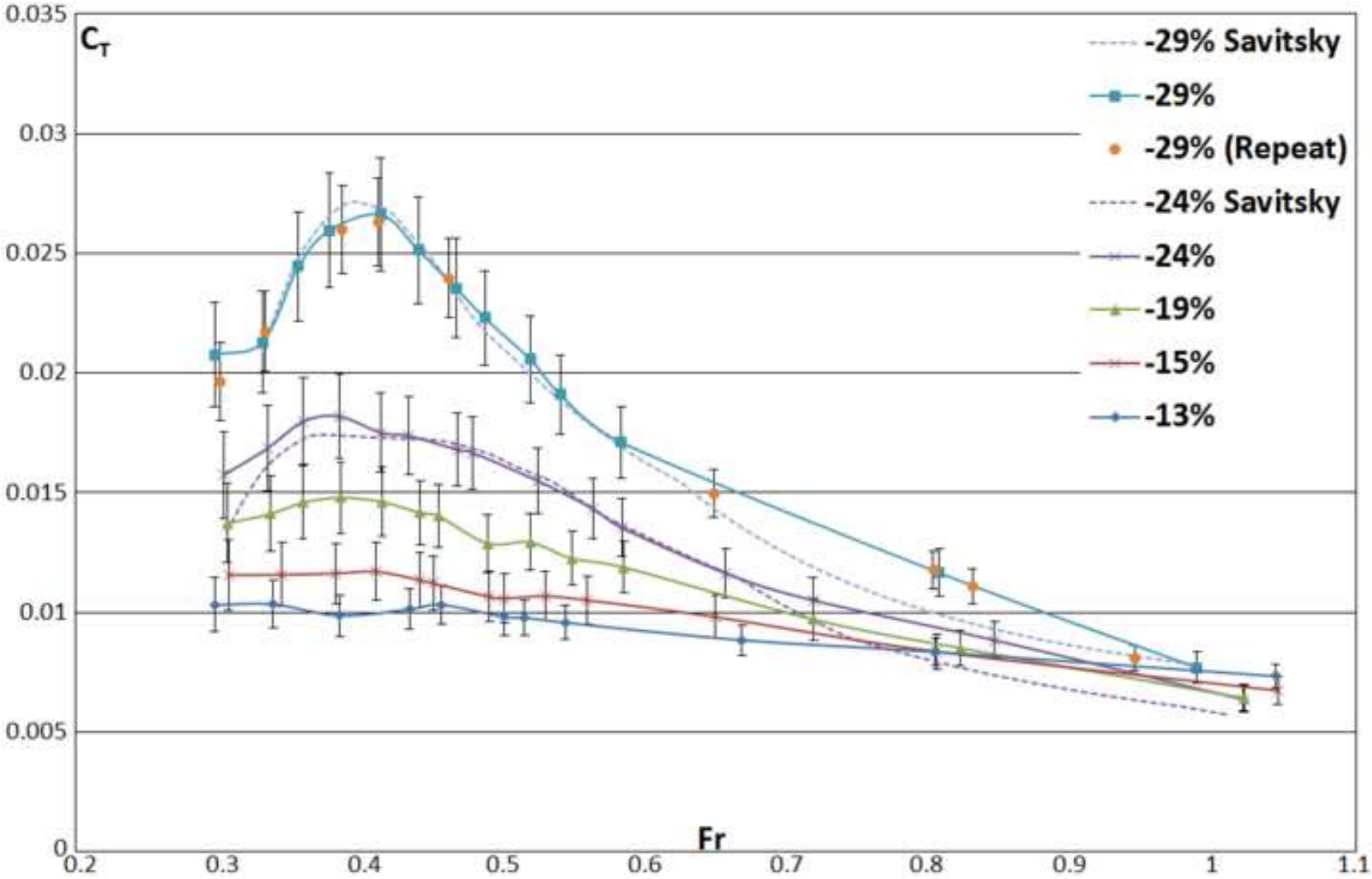

Figure 10
Click here to download high resolution image

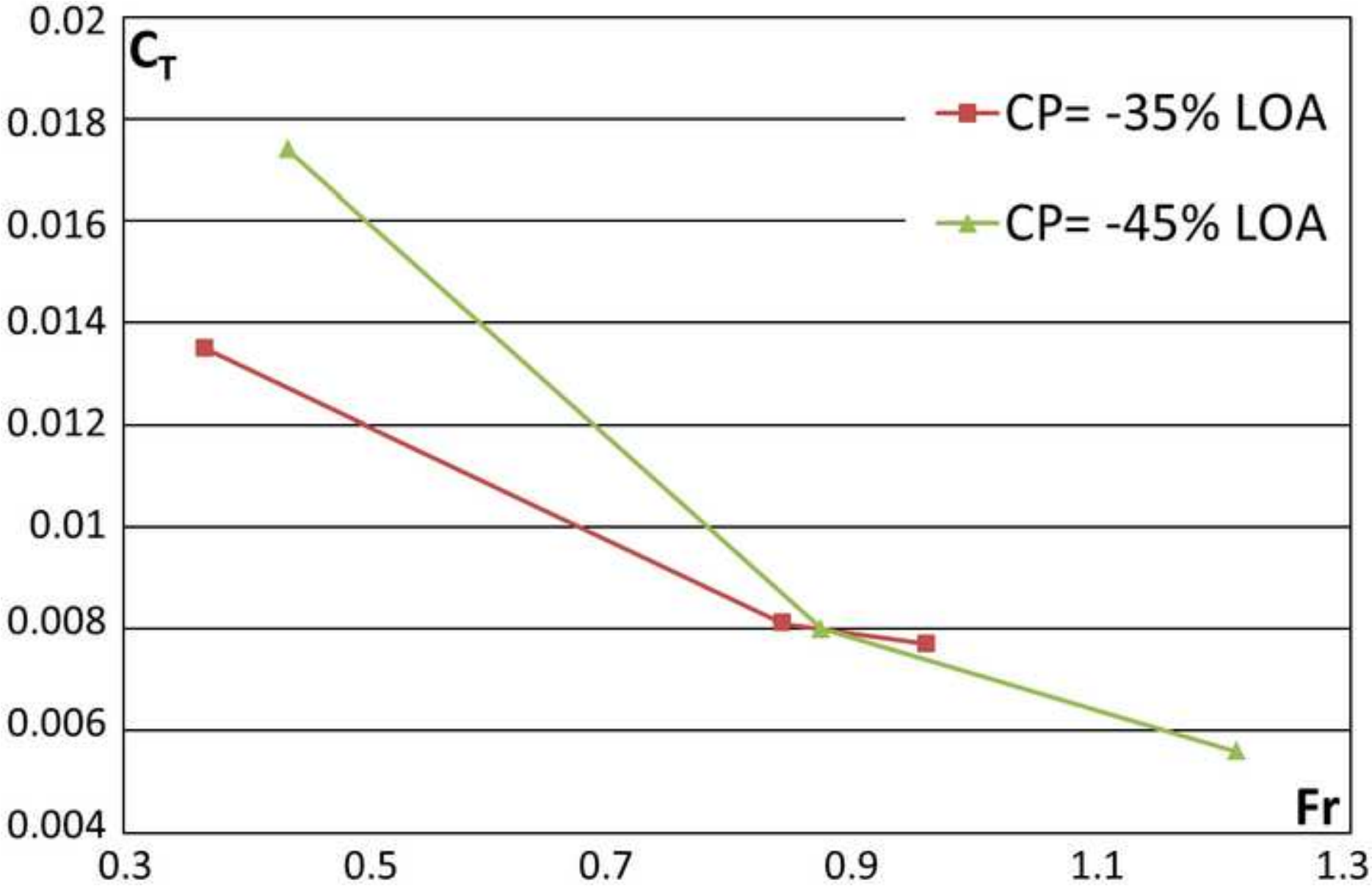

Figure 11
Click here to download high resolution image

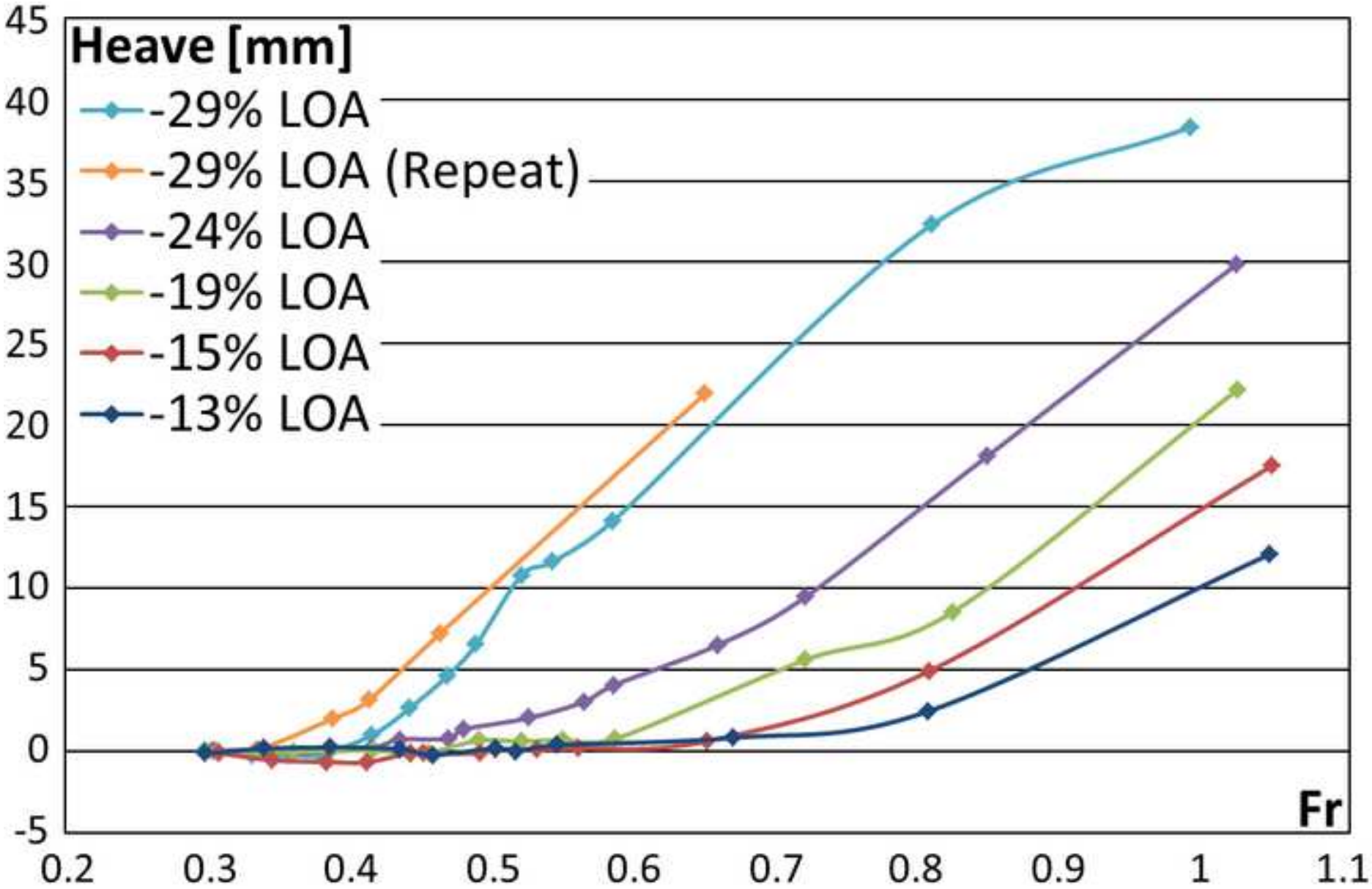

Figure 12
Click here to download high resolution image

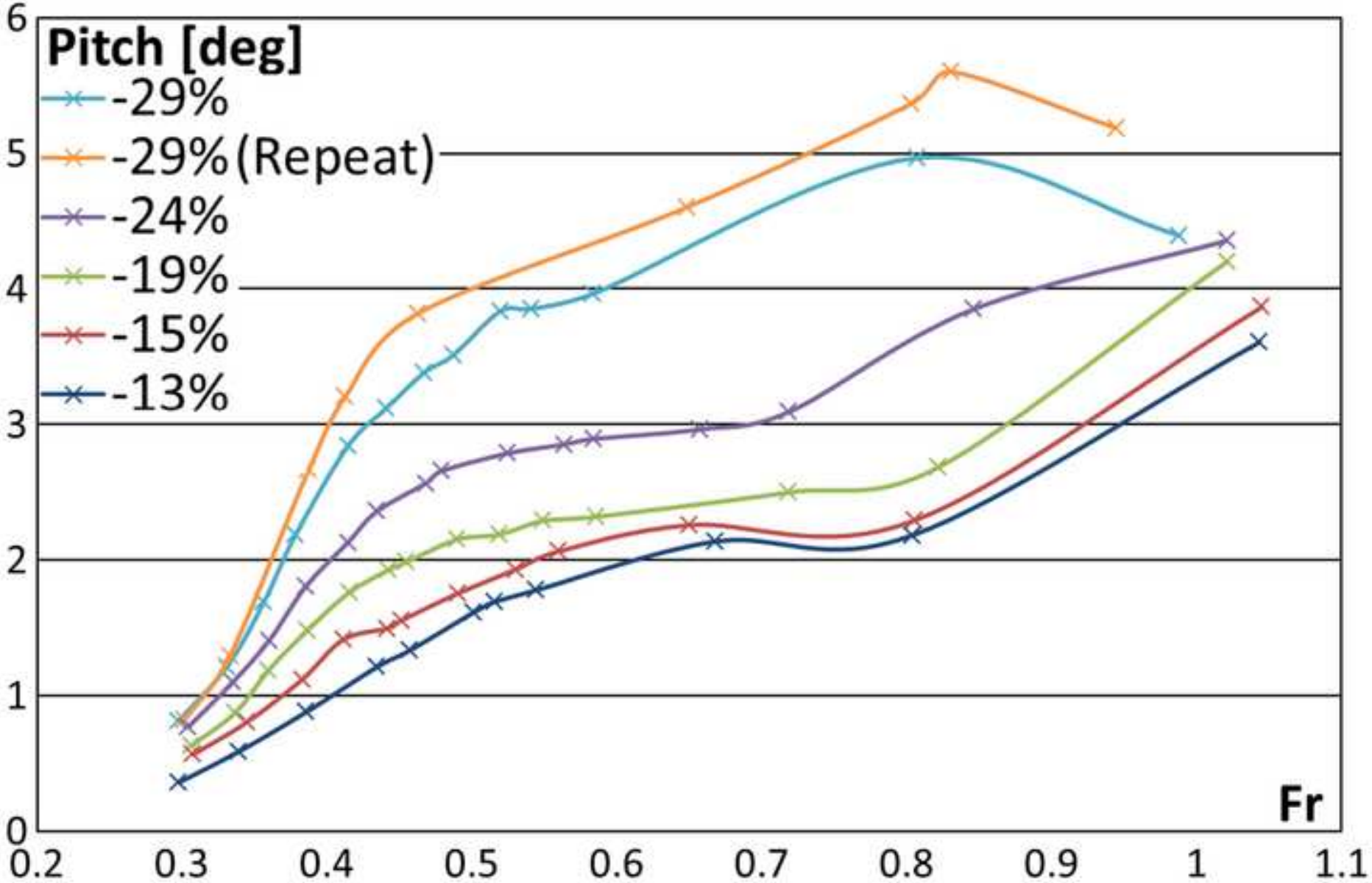

Table

Table 1: Weights breakdown.

Item	Weight [kg]
Model	1.794
Gifford dynamometer & heave post	4.609
Ballast	2
Total	8.403
Counterweight	-4.862
Model-scale still-water displacement	3.541

Table 2: Ballast positions and resulting LCG and LWL (model scale).

Ballast Position [%LOA from MS, +fwd]	**LCG [%LOA from MS, +fwd]**	**LWL [m]**
-17	-13	1.16
-21	-15	1.11
-29	-19	1.07
-36	-24	1.03
-46	-29	1.00

Table 3: V and Fr (based on LOA) tested for each test condition.

	LCG [%LOA from MS, +fwd]					
$V\ [m/s]/Fr[-]$	**-13**	**-15**	**-19**	**-24**	**-29**	**-29**
	$1.02/0.30$	$1.06/0.31$	$1.05/0.31$	$1.04/0.30$	$1.02/0.30$	$1.04/0.30$
	$1.16/0.34$	$1.18/0.34$	$1.16/0.34$	$1.15/0.33$	$1.14/0.33$	$1.14/0.33$
	$1.32/0.39$	$1.31/0.38$	$1.23/0.36$	$1.24/0.36$	$1.22/0.36$	$1.33/0.39$
	$1.49/0.43$	$1.41/0.41$	$1.33/0.39$	$1.32/0.39$	$1.30/0.38$	$1.42/0.41$
	$1.57/0.46$	$1.52/0.44$	$1.43/0.42$	$1.42/0.41$	$1.42/0.41$	$1.59/0.46$
	$1.72/0.50$	$1.55/0.45$	$1.52/0.44$	$1.49/0.43$	$1.51/0.44$	$2.22/0.65$
	$1.77/0.52$	$1.68/0.49$	$1.56/0.45$	$1.61/0.47$	$1.60/0.47$	$2.75/0.80$
	$1.87/0.54$	$1.72/0.50$	$1.68/0.49$	$1.64/0.48$	$1.67/0.49$	$2.85/0.83$
	$2.29/0.67$	$1.82/0.53$	$1.78/0.51$	$1.80/0.52$	$1.78/0.52$	$3.24/0.94$
	$2.76/0.80$	$1.92/0.56$	$1.88/0.55$	$1.93/0.56$	$1.86/0.54$	
	$3.58/1.04$	$2.23/0.65$	$2.01/0.59$	$2.00/0.58$	$2.00/0.58$	
		$2.76/0.80$	$2.47/0.72$	$2.25/0.66$	$2.77/0.81$	
		$3.59/1.05$	$2.82/0.82$	$2.46/0.72$	$3.39/0.99$	
			$3.50/1.02$	$2.90/0.84$		
				$3.50/1.03$		

Table 4: Uncertainty analysis for a test run at $1.8\ \mathrm{m/s}$ and a $LCG = -24\%$.

Wetted surface, S	**0.182 m^2**	
$U_{S,MOD}$	1.817·10^{-3} m^2	0.996%
$U_{S,BAL}$	2.002·10^{-5} m^2	0.011%
U_S	1.817·10^{-3} m^2	0.996%
Velocity, V	**1.800 m/s**	
$U_{V,CAL}$	5.150·10^{-5} m/s	0.005%
$U_{V,DAQ}$	1.487·10^{-4} m/s	0.008%
U_V	1.698·10^{-4} m/s	0.009%
Resistance, R_T	**4.514 N**	
$U_{R_T,CAL}$	4.514·10^{-5} N	0.001%
$U_{R_T,FIT}$	3.370·10^{-2} N	0.747%
$U_{R_T,DAQ}$	2.444·10^{-1} N	5.416%
$U_{R_T,MIS}$	6.820·10^{-1} N	1.511%
U_{R_T}	2.560·10^{-1} N	5.672%
Density	**998.84 kg/m^3**	
t	20°C	
U_t	0.75°C	3.75%
U_ρ	0.2943 kg/m^3	0.03%
Resistance coefficient, C_T	**1.550·10^{-2}**	
U_{C_T}	1.706·10^{-3}	11%

Table 5: Sensitivities.

i	δi [%]	δC_T [%]	θ_i
R_T	22.16	18.14	0.82
ρ	0.10	-0.10	-1.00
S	555.56	-555.56	-1.00
V	55.56	-141.98	-2.56

Table 6: Cross-overs of minimum C_T conditions.

LCG	From	
[$\%LOA$]	Fr	C_t
-13	-	-
-15	0.81	8.3
-19	0.91	7.6
-24	1.0	6.6
-29	1.09	5.3

Captions

Figure 1: Mathematical model of the Aura and her full-scale dimensions

Figure 2: Photograph of the Aura in full scale with an aft crew position.

Figure 3: Photograph of the Aura in full scale with a forwards crew position.

Figure 4: Photograph of the Aura 1:4 model in the towing tank.

Figure 5: Experimental Setup.

Figure 6: Gifford dynamometer.

Figure 7: Surface plot of R_T versus LCG for a range of V.

Figure 8: Prohaska plot.

Figure 9: C_T versus Fr for different LCG.

Figure 10: Optimum crew position for different Froude numbers.

Figure 11: Heave versus Fr for different LCG.

Figure 12: Pitch versus Fr for different LCG.

Table 1: Weights breakdown.

Table 2: Ballast positions and resulting LCG and LWL (model scale).

Table 3: V and Fr (based on LOA) tested for each test condition.

Table 4: Uncertainty analysis for a test run at $1.8\ \mathrm{m/s}$ and a $LCG = -24\%$.

Table 5: Sensitivities.

Table 6: Cross-overs of minimum C_T conditions.